International Journal of Engineering and Technology Innovation, vol. 5, no. 3, 2015, pp. 178-188

Aero Acoustic Noise Analysis of a Locomotive Cooling System Ducts and Structure Optimization

Shan-Shan Li [1,*], Ming Li[1, 2], Fan Yang[3], Jun-Fang Li[1], Kan Wang[1]

[1]College of Automotive Engineering, Jilin University, Changchun 130025, China.

[2]State Key Lab. of Automotive Simulation and Control, Jilin University, Changchun 130025, China.

[3]Dalian Locomotive and rolling stock co., Ltd. CNR group, Dalian 116022, China.

Received 31 March 2015; received in revised form 03 August 2015; accepted 06 August 2015

Abstract

Aero acoustic noise of a locomotive cab cooling system ducts was analyzed by method of Computational Fluid Dynamics (CFD) and Computational Aero acoustic (CAA) approach. Flow characteristic of the ducts was analyzed by CFD software, then near-field and far-field aero acoustic noise was forecasted with BNS model and FW-H model respectively. Duct structure was optimized according to the analysis of flow field and sound field. Results indicated that noise characteristic of sensitive frequency band at the position of human ear with the optimized duct has a significant improvement.

Keyword: Flow field analysis, Aero acoustic analysis, BNS model, FW-H model

1. Introduction

Recently, locomotives take an important role in modern transportation. Like automotive, aero acoustic noise outside high-speed train is significant, aroused the attention of scholars at home and abroad. Sha Huang [1] found that the curvature of train head surface has significant influence on surface fluctuating pressure, aero acoustic noise can be reduced by changing the head design of streamline shape. J. Munoz- Paniagua [2] improved the train aerodynamic by changing train head parameters, thereby reducing the aero acoustic noise. These researches are focused on train head shape parameters, they only have connections with train external aeroacoustics. Due to the poor sealing of the locomotive cab operations console, high-speed air flows into cab through the gap at the operations console, combined with aero acoustic noise from cooling system, worsened indoor air noise environment of locomotive cab. Poor noise environments not only make drivers feel uncomfortable, but also distract them, or even worse, reduce driving safety and endanger the lives of drivers and crews. It is very important to research and control the locomotive cab noise environment.

Predictive tools for the aero acoustic behavior of components, subsystems and whole systems early on in the design phase are therefore desirable. With the development of computational fluid dynamics and aero acoustics, the study on fluid aerodynamic noise with the numerical method has become possible. Currently, research method of fluid aerodynamic noise mainly includes direct noise simulation, sound analogy, broadband noise source model method, CFD software and professional acoustic code coupling method. The ability of an analysis tool to characterize a system's level of noise and its spectral distribution at a receiver location is a powerful design tool. It could be used as a virtual test lab to measure whether a given

* Corresponding author. E-mail: lss13@mails.jlu.edu.cn

system meets its design requirements. Currently, such capability is not available within a development cycle for complex industrial applications. This is due to the fact that noise information at receiver locations requires the solution of both the flow field and the acoustic field. However, during early stages of the product development, noise information at receiver locations is not critical. Rather, reliable system noise information at the source may be sufficient to provide design direction during development. Noise information at the source requires only a CFD solution that captures unsteady flow structure. At early stages of the development cycle, a CFD tool that provides a measure of noise levels at the source for a given system in order to provide a design direction would be very useful. In addition, if that tool is able to identify components or surfaces that generate most of the noise it would provide, to the development team, a valuable means to derive design optimization.

In this paper, a numerical simulation on a locomotive cab was performed to analyze the distribution of the flow field. Then the noise prediction was performed on the basis of the flow field results to find out the distribution of the noise source with broadband noise source model and the radiation characteristics of the noise source with FW-H sound analogy method. At last, optimization of the duct structure was performed, which provided a theoretical basis for the cab's acoustic environment improvement.

2. Model and Boundary Condition

Here, a case will be studied where the initial level design of a locomotive cab cooling system duct did not meet its design requirements due to high levels of NVH, poor overall sound quality, and poor airflow distribution of outlet. The three-dimensional model of the cooling system duct was created with CATIA software, as shown in Fig.1 (a). The duct model grids were meshed by polyhedral mesh for its geometric adaptability, and the air inlet and air outlet were refined accordingly. Extruder mesh was selected at duct inlet and outlets to increase fluid stability and avoid unnecessary reverse flow, adverse to flow field analysis results, in turn affecting the sound field analysis result correctness. The final mesh model was shown in Fig.1 (b).

(a) Geometric model (b) Model grids

Fig. 1 Duct solid model

The duct inlet was set as mass flow inlet, and the value of mass flow was 0.23 Kg/s, according to the design specifications. Because the duct outlet is vented to the atmosphere, the duct outlet was set as pressure outlet.

3. Flow Field Calculation

3.1 Fluid field analysis model

Flow field analysis was based on the Reynolds-averaged Navier-Stokes model (RANS). The Realizable K-E model was to solve the N-S equations, to obtain the average flow field information throughout the process.

A formula for turbulent viscosity and a transport equation for turbulent dissipation rate are added to the Realizable K-E

model, making this model has a good performance in analysis on flow separation and complex secondary flow. Based on the theory of computational fluid dynamics analysis [3], the transport equations for the realizable K-Epsilon model are shown by Eqs. (1) and (2):

$$\frac{d}{dt}\int_V \rho k dV + \int_A \rho k(\vec{v}-\vec{v}_g)\cdot d\vec{a} = \int_A (\mu + \frac{\mu_t}{\sigma_k})\nabla k \cdot d\vec{a} + \int_V [G_k + G_b - \rho((\varepsilon - \varepsilon_0) + \gamma_M) + S_k] dV \tag{1}$$

$$\frac{d}{dt}\int_V \rho \varepsilon dV + \int_A \rho \varepsilon(\vec{v}-\vec{v}_g)\cdot d\vec{a} = \int_A (\mu + \frac{\mu_t}{\sigma_\varepsilon})\nabla \varepsilon \cdot d\vec{a} + \int_V \left[C_{\varepsilon 1} S\varepsilon + \frac{\varepsilon}{k}(C_{\varepsilon 1} C_{\varepsilon 3} G_b) - \frac{\varepsilon}{k+\sqrt{v\varepsilon}} C_{\varepsilon 2}\rho(\varepsilon - \varepsilon_0) + S_\varepsilon \right] dV \tag{2}$$

where S_κ and S_ε are the user-specified source terms, W/m^3; $\mathcal{E}_0$ is the ambient turbulence value in the source terms that counteracts turbulence decay, J/kg; S is the modulus of the mean strain rate tensor, γ_M is the dilatation dissipation, m^2/s^3; μ is the dynamic viscosity, m^2/s; μ_t is The turbulent viscosity, m^2/s; $C_{\varepsilon 1}$, $C_{\varepsilon 2}$ and σ_κ are model coefficients, G_b and G_κ are turbulent production, J/kg.

3.2 Flow field results analysis

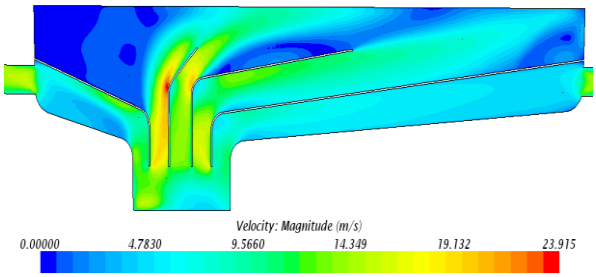

Fig. 2 Duct baffle area velocity cloud

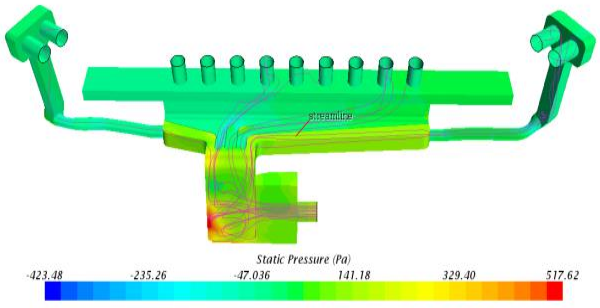

Fig. 3 Duct static pressure contours and streamline

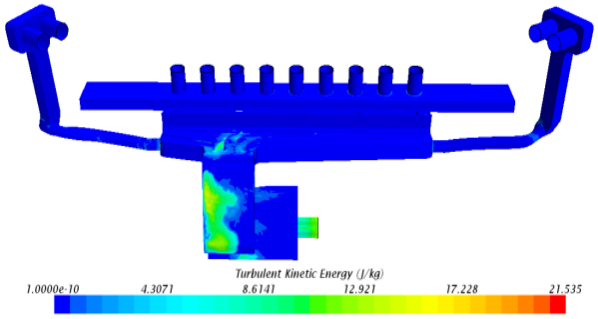

Fig. 4 Duct turbulent kinetic energy contours

It can be seen from Figs. 2 - 4 that the maximum velocity place located at baffle expansion area, and the maximum velocity value was 23.940 m/s, the static variation amplitude was 941.1 Pa, the maximum turbulent kinetic energy was 23.535 J/kg. The Mach number of the duct is less than 0.3, for the maximum velocity is less than 102 m/s, it can be inferred that the dipole noise was the main noise source. The duct streamline indicated that airflow distribution of duct outlets is poor, it is also a factor affecting the duct aeroacoustics.

Figs. 2- 4 show that the high-speed fluid flows into duct vertical section through the trapezoid body, and hits the surface of the duct at the corner, which results in the fluid velocity changes, and disturbances get severe, and turbulent kinetic energy increases, and the static pressure increases. When fluid reaches the baffle area, the velocity of fluid around the corner increases,

negative pressure region emerges, and vortex forms, so that the unevenness of the distribution of the internal fluid duct phenomenon is more obvious, and the flow disturbance and turbulent energy dissipation are more serious. Severe fluid disturbance increases fluid flow resistance, which causes energy loss, wherein part of the energy will propagates outward in the form of acoustic energy, Jian-Peng Yao said in his paper [4], and generates noise.

3.3 Near-field noise prediction model

The noise source prediction was made with broadband noise source models (BNS) which has been recognized by domestic and foreign scholars like Zheng-Yu Zheng [5], A. Zanon [6] and Fred Mendonca [7]. Broadband noise source model is mainly divided into four models:

(1) Curle noise source model

The Curle Noise source model evaluates the noise from a turbulent boundary layer flow over a solid body at low Mach number. The model represents dipole sources of noise coming from the fluctuating surface pressure from solid boundaries acting on the fluid. Specifically, this model computes the surface acoustic power to evaluate the local contribution to the total acoustic power per unit area of the body surface. C. Schram [8] showed the Curle surface integral by eq. (3):

$$p'(\vec{x},t)=\frac{1}{4\pi a_0^3}\int_S\left[\frac{(\vec{x}-\vec{y})}{r^2}\frac{\partial p}{\partial t}\left(\vec{y},t-\frac{r}{a_0}\right)\right]\vec{n}dS(\vec{y}) \tag{3}$$

where $t-\frac{r}{a_0}$ is the emission time(s), p is the surface pressure, (Pa), $\acute{p}$ is the acoustic pressure, (Pa), a_0 is the far-field sound speed, (m/s).

(2) Lilley Noise source model

The Lilley equation computes the quadrupole noise from the fluctuating velocity flow field. Applications include problems where local shear effects dominate, such as flow around solid bodies and shear flows in channels. David W. Wundrow [9] showed the Lilley equation for problems without heat transfer as eq. (4):

$$\frac{d}{dt}\left[\frac{d^2\Pi}{dt^2}-\frac{\partial}{\partial x_j}\left(a^2\frac{\partial\Pi}{\partial x_j}\right)\right]+2\left[\frac{\partial u_k}{\partial x_j}\frac{\partial}{\partial x_k}\right]\left(a^2\frac{\partial\Pi}{\partial x_j}\right)=-2\left[\frac{\partial u_k}{\partial x_i}\frac{\partial u_j}{\partial x_k}\frac{\partial u_i}{\partial x_j}\right] \tag{4}$$

where a is the speed of sound, (m/s), ∂_{ik} is the stress tensor.

(3) Linearized Euler Equation noise source model

The Linearized Euler Equations (LEE) account for refraction and convection effects in any sheared mean flows. It can be used to compute the quadrupole noise for a wider range of conditions than the Lilley equation, in which the associated source term is a nonlinear function of the fluctuating velocity flow field. Takuya Oshima Imano [10] showed the LEE equation as Eqs. (5)-(7):

$$p_i(\vec{x},t)=P_i(x)+p_i'(\vec{x},t)+p_{ai}(\vec{x},t) \tag{5}$$

$$u_i(\vec{x},t) = U_i(x) + u_i'(\vec{x},t) + u_{ai}(\vec{x},t) \tag{6}$$

$$\rho_i(\vec{x},t) = \overline{\rho}_i(x) + \rho_i'(\vec{x},t) + \rho_{ai}(\vec{x},t) \tag{7}$$

where the acoustic components p_{ai}, u_{ai} and ρ_{ai} are small compared to the mean components P_i, U_i and $\overline{\rho}_i$ and the turbulent components p_i', u_i' and. ρ_i'

(4) Proudman noise source model

The Proudman noise source model evaluates acoustic power per unit volume, and the sound is from quadrupoles. Specifically, this model computes the acoustic power to evaluate the local contribution to the total acoustic power per unit volume from the turbulent flow. This model has been used for rotating parts, heat exchangers and distribution ducts. S. Sarkar [11] showed the local acoustic power generated by unit volume of isotropic turbulence by Eq. (8):

$$AP = \alpha\rho_0 \frac{u^3}{l}\frac{u^5}{a_0^5} \tag{8}$$

where α is a constant related to the shape of the longitudinal velocity correlation, u is the root mean square of one of the velocity components, (m/s) l is the longitudinal integral length scale of the velocity, (m), ρ_0 is the far-field density (kg/m^3), and a_0 is the far-field sound speed, (m/s).

3.4 Near-field noise prediction results

Curle noise source model was chosen to analyze duct surface dipole noise, Proudman noise source model was chosen to analyze duct volume quadrupole noise for the reason that it has been well used in distribution duct applications and it can be easily recognized by using unit dB, not /s^3 for Lilley and m/s^2 for LEE. These two models based on Lighthill's analogy, require little computational effort in extracting, from a steady state CFD solution, the Acoustic Power (AP) and the Surface Acoustic Power (SAP). Both aeroacoustic variables are accessed within the Fluent Solver as an aeroacoustic post-processing tool. AP provides Proudman's quadrupole noise generation, whereas SAP provides Curle's surface dipole noise generation. These two aeroacoustic variables are well suited to Air Handling Subsystem (AHS) applications which represent a complex internal flow that includes rotating parts (blowers), heat exchangers, and distribution ducts. In these low Mach number flows, surface dipole noise radiation generally contributes most of the system noise. The location and strength of noise sources are shown as Figs. 5-7.

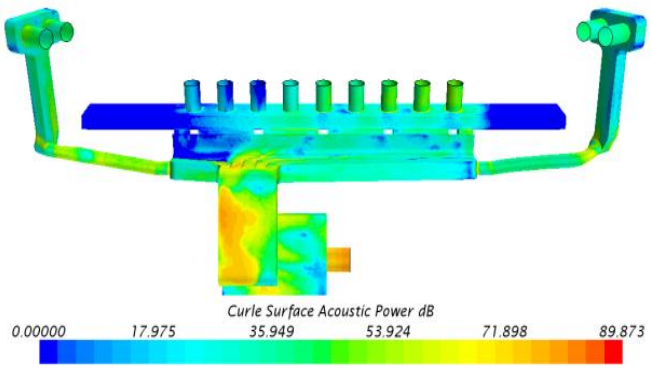

Fig. 5 Duct surface dipole noise source distribution

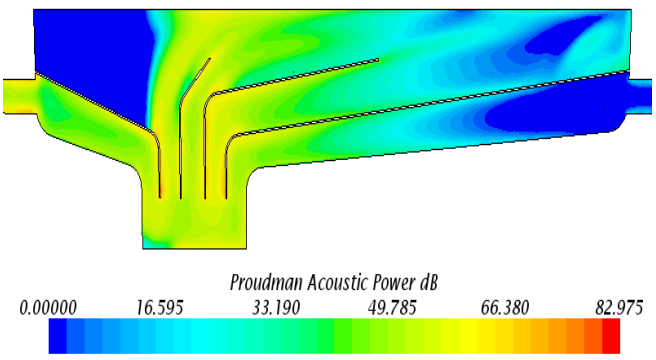

Fig. 6 Duct baffle area quadrupole noise source distribution

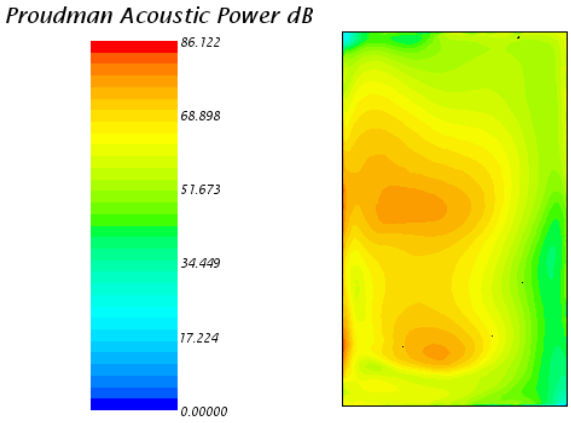

Fig. 7 Duct vertical section quadrupole noise source distribution

Figs. 5-7 show that duct vertical section and baffle areas were main dipole noise sources and quadrupole noise sources, the dipole noise at these two places were 89.873 dB and 82.975 dB, the quadrupole noise at these two place were about 70 dB and 65 dB. The quadrupole noise was largely less than dipole noise, it can be concluded that the dipole noise is the main noise source. Meanwhile, these places are also the turbulence areas from results of flow field. This indicates that disturbance areas propagate acoustic energy.

BNS models do not provide any tonal noise information or noise spectra at receiver locations. Instead they provide only the location of noise source and an approximate measure of the radiated noise at the source. For quantifying the result, further analysis should be performed to obtain noise spectra at receiver locations. All previous approaches required a transient CFD solution that captures the flow structure and presents some challenge in terms of resource requirements and solution time. Although the coupled approach is within reach for automotive applications, it cannot be incorporated, at the present, into a fast paced development process.

4. Unsteady state calculation

4.1 Time step

Unsteady state calculation was carried out after steady state calculation gets stable, and the large eddy simulation model (LES) was used to solve the fluid instantaneous information. The time step can be calculated as equation (9):

$$f = \frac{1}{\lambda} = \frac{1}{2\Delta t} \tag{9}$$

where f is the frequency expected, Hz; Δt is the time step, s. Take 5000 Hz as the frequency in this paper, then the time step is 0.0001 s.

Based on the theory of computational fluid dynamics analysis [3], the transport equations for the LES model are shown by Eqs. (10) and (11):

$$\frac{\partial \rho}{\partial t} + \frac{\partial \rho \vec{u}_i}{\partial x_i} = 0 \tag{10}$$

$$\frac{\partial}{\partial t}(\rho\bar{u}_i)+\frac{\partial}{\partial x_j}(\rho\bar{u}_i\bar{u}_j)=\frac{\partial}{\partial x_j}(\mu\frac{\partial\sigma_{ij}}{\partial x_j})-\frac{\partial\bar{p}}{\partial x_i}-\frac{\partial\tau_{ij}}{\partial x_j} \tag{11}$$

where $\bar{u}_i$ and $\bar{u}_j$ are the filtered velocity component, (m/s), μ is the turbulent viscosity, (m^2/s), $\bar{p}$ is the pressure, (Pa), σ_{ij} is the viscous stress tensor (Pa), τ_{ij} is the sub grid stress, (Pa).

4.2 Far-field noise prediction model

Sound analogies are based on a reformulation of the basic governing flow equations, the compressible Navier-Stokes equations. Rearranged, these equations yield an inhomogeneous wave equation with source terms on the right hand side. With some assumptions, the equation expresses a linear wave problem in a medium at rest with the equivalent acoustic sources like monopoles, dipoles, and quadrupoles derived from the transient flow field predicted in CFD. Due to the transformation of the aeroacoustic problem into a problem of classical acoustics, it is called sound analogy.

FW-H sound analogy model was added during the unsteady state calculation for its widely used. Duct surface was selected as FW-H surfaces, derived points around driver ears, call them left point and right point, was created as FW-H receivers. Sampling time was started from 0.03s to 0.1s. M. Gennaro [12] showed the control equation for FW-H acoustic model as equation (12):

$$\left[\frac{1}{c_0^2}\frac{\partial^2}{\partial t^2}-\frac{\partial^2}{\partial x_i^2}\right]p'=\frac{\partial}{\partial t}\left[\rho v_n\delta(f)\nabla f\right]-\frac{\partial}{\partial x_i}\left[n_i p\delta(f)\nabla f\right]+\frac{\partial^2}{\partial x_i\partial x_j}\left[T_{ij}H(f)\right] \tag{12}$$

where p' is the sound pressure, (Pa), n_i is the surface normal vector, v_n is the surface velocity component normal to the surface, (m/s), the right three respectively represent the monopole, dipole and quadrupole source.

4.3 Monitoring points

In order to further understand the characteristics of the noise generation and radiation, monitoring points were set at duct internal turbulent flow region and drivers ear position respectively. The fluid instantaneous information of these points was monitored using LES solver during the analysis, and the FW-H solver transfer the pressure fluctuation information using Fast Fourier Transform (FFT) method. The position of the monitoring points is shown in Fig. 8.

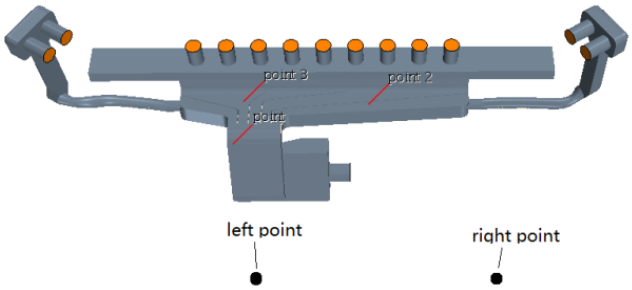

Fig. 8 The position of the monitoring points

4.4 Far-field noise prediction results

Fig. 9 indicates that the noise duct surface produced has no obvious peak in the whole frequency band, which means as the noise that the duct surface generated is broadband noise, and it is accurate to use the broadband noise source model (BNS) for noise prediction. In addition, duct noise can be reduced by changing duct geometrical structure.

The sound pressure level ranges from 40 dB to 120 dB near 70 Hz. In the whole frequency band, sound pressure level at vertical section monitoring point 1 is maximum, its sound pressure level ranges from 60 dB to 122 dB, sound pressure level at baffle area monitoring point 3 is moderate, its sound pressure level ranges from 50 dB to 118 dB, and sound pressure level at baffle area monitoring point 2 is minimum, its sound pressure level ranges from 40 dB to 110 dB. This indicates that duct vertical section's pulsation is most intense and it is the main noise source, which relative to the flow field results and BNS prediction results, and noise reduction in this region is the focus of the work.

Fig. 10 indicates the spectral distribution around the left and right drivers' ear position are almost in same. The entire sound pressure band value ranges from 15 dB near 1800 Hz to 57 dB near 80 Hz. The sound pressure in the low frequency region is normally above 40 dB, and the sound pressure in medium high frequency region is between 20 - 40 dB. Qiang Gu [13] said in his book that humans sensitive frequency band is 2000 - 4000 Hz, duct sound pressure level in this band is about 32 dB.

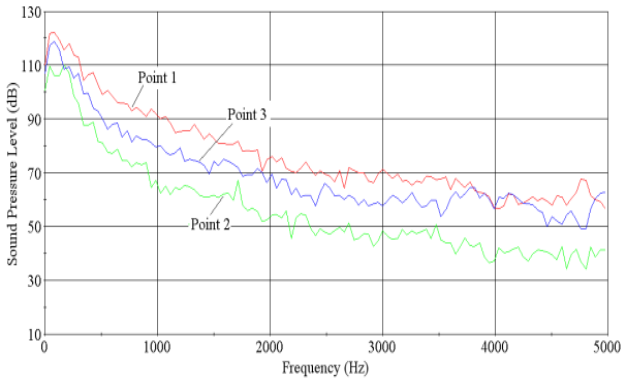

Fig. 9 Sound spectrum for original duct internal monitor points

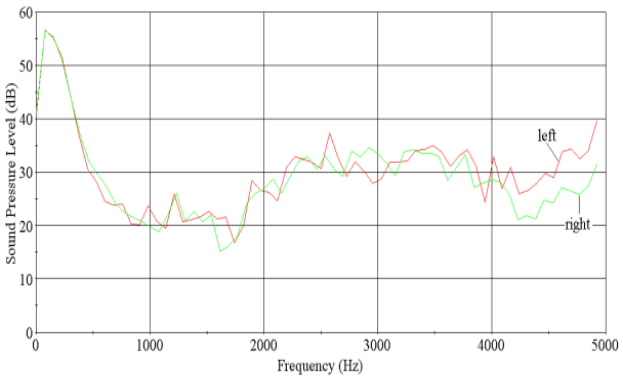

Fig. 10 Original duct sound spectrum for driver ears

5. Controlling duct aero acoustic noise

5.1 Optimizing duct geometry structure

The analysis results of the flow field and the sound field of the original duct indicate that the vertical section is the main source generating aero acoustic noise, and the sound field is related to flow field, so general flow field improved measurement can be taken to improve sound field. Because the connection structure of trapezoid body and vertical section changes suddenly, high speed airflow flows through here and the speed direction and magnitude changes dramatically, which produces a severe disturbance that forms the aerodynamic noise. Duct connection structure was optimized with a round corner to improve the aero acoustic characteristics. Original and Improved structures are shown in Fig. 11 (a) and (b) respectively.

(a) Original (b) optimized

Fig. 11 Trapezoid structure schematic

5.2 Flow field results analysis

The Realizable K-E model was used for the optimized duct flow field analysis, and the average flow field information throughout the process was obtained. The flow field distribution was shown as Figs. 12 - 14.

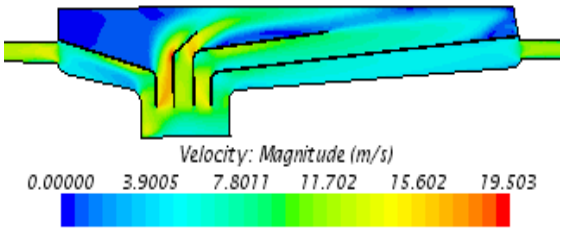

Fig. 12 Duct baffle area velocity cloud

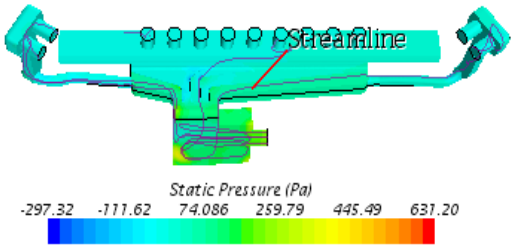

Fig. 13 Duct static pressure contours and streamline

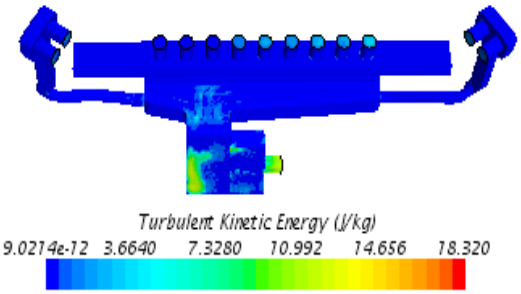

Fig.14 Duct turbulent kinetic energy contours

It can be seen from Figs. 12-14 that the optimized duct maximum velocity of duct baffle area was 19.503 m/s, the static variation amplitude was 928.52 Pa, and the maximum turbulent kinetic energy was 18.320 J/kg. Compared with the initial duct, the main flow field characters of the optimized duct were all reduced, indicated that the optimized duct flow field was improved.

5.3 Noise prediction results

Curle and Proudman sound models were used to analyze the approximate sound field for the optimized duct. Same monitoring points were arranged. Optimized duct near-field noise prediction results are shown with Fig. 15 - Fig. 17. Sound spectral curves are shown as Figs. 18-19.

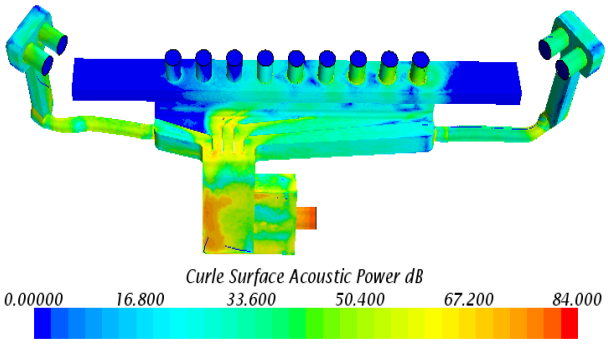

Fig. 15 Duct surface dipole noise source distribution

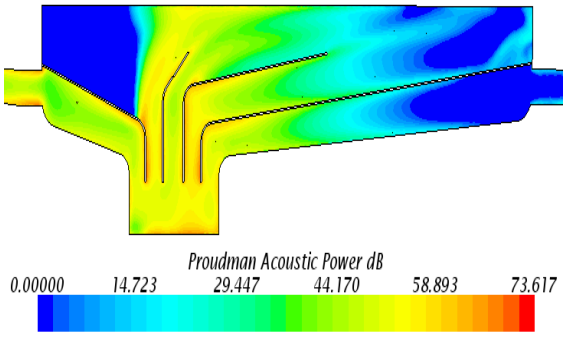

Fig. 16 Duct baffle area quadrupole noise source distribution

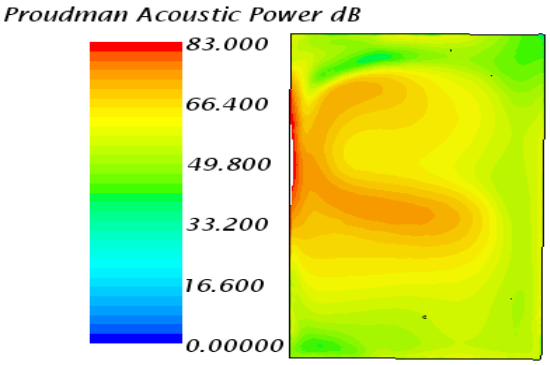

Fig. 17 Duct vertical section quadrupole noise source distribution

It can be seen that the dipole noise at vertical section area and duct baffle area of the optimized duct were 84 dB and 73.617 dB, the quadrupole noise at these two places were about 70 dB and 56 dB. Compared Figs. 5-7 with Figs. 15-17 that optimized duct dipole noise decreased about 7 dB than original duct, and the quadrupole noise decreased about 5 dB. The size of noise source is smaller than original duct. The intensity of the noise source is smaller than original duct. These indicated that the sound field of the duct was improved from changing the duct structure.

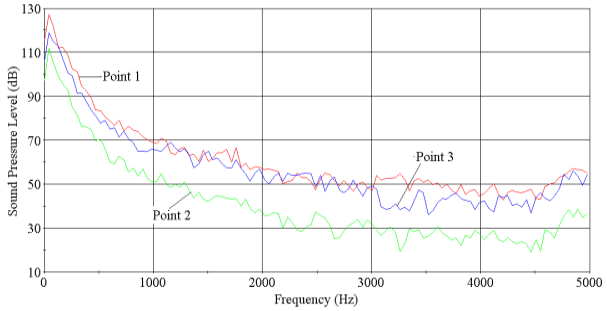

Fig. 18 Sound spectrum for optimized duct internal monitor points

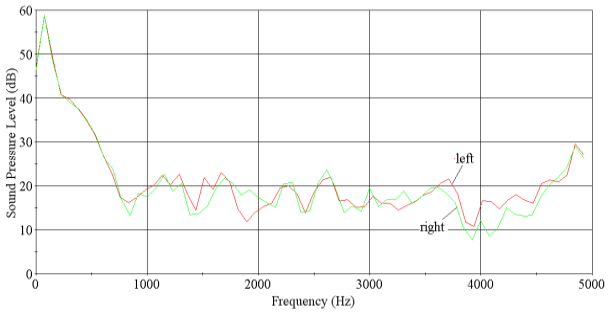

Fig. 19 Optimized duct sound spectrum for driver ears

It can be seen from Fig. 18 that sound pressure level at vertical section monitoring point 1 ranges from 128 dB to 50 dB, sound pressure level at baffle area monitoring point 3 ranges from 120 dB to 40 dB, and sound pressure level at baffle area monitoring point 2 ranges from 110 dB to 20 dB. Comparing Fig. 9 with Fig. 15, the sound pressure level of each monitoring point has decreased after the modification, in which the monitor 1 decreased most obvious, and the sound pressure level decreased in the high frequency band significantly. Although their maximum sound pressure level increase, at such low frequency band about 70 Hz, it can be neglect.

It can be seen from Fig. 19 that sound pressure level near drives ears ranges from 57 dB to 10 dB. Comparing Fig. 10 with Fig. 16, the sound pressure level of the optimized duct is about 17 dB at humans sensitive frequency band, lower than the sound pressure level of the original duct 32 dB for 15 dB, the noise reduce effect is obvious.

6. Conclusion

In this paper, a combined CFD and CA approach for the numerical prediction of flow-induced noise in a locomotive cab cooling system ducts is investigated. The so-called CAA approach consists of two main parts: a CFD calculation of the flow field for the determination of sound sources, and the CA calculation of the sound prediction and sound propagation to obtain the resulting sound field.

Analysis results show that Broadband noise source models (BNS) can effectively predict the location of duct noise source, and provide a basis for optimization the noise characteristics of the duct. For the optimized duct structure, high frequency sound pressure level decreases 15dB, and the noise reduce effect is obvious. In order to reduce the aero acoustic noise, it is necessary to reduce structural breaks, and the connection between various structures should be optimized to reduce the degree of airflow disturbance.

Although the presented results show good performance, further analyses are needed to investigate more closely the several boundary conditions used for the numerical simulation with CFD and CA.

References

[1] S. Huang, Research on numerical simulation of aerodynamic noise outside the high-speed train, Master Thesis, Graduate School of Vehicle Movement Engineering, Central South University, 2009. (In Chinese)
[2] J. Munoz-Paniagua, J. Garcia and A. Crespo, "Genetically aerodynamic optimization of the nose shape of a high-speed train entering A tunnel," Journal of wind engineering and industrial aerodynamics, vol. 130, pp. 48-61, May 2014.
[3] F. J. Wang, Computational fluid dynamics analysis, 1st ed. Beijing: Tsinghua University Press, 2004. (In Chinese)
[4] J. P. Yao, "Calculation analysis and control for air conditioning system aerodynamic noise of a medium bus," Jilin Univ., Graduate School of Automotive Eng., Master Thesis, China, 2012. (In Chinese)
[5] Z. Y. Zheng, "A study on the numerical simulation of high-speed vehicle's external aerodynamic acoustic field," Doctoral Thesis, Graduate School of Vehicle Eng., Southwest Jiaotong Univ., China, 2012. (In Chinese)
[6] A. Zanon, M. De Gennaro, H. Kuehnelt, D. Langmayr, and D. Caridi, "Investigation on the influence of mesh topology and free stream turbulence intensity in broadband noise prediction of axial fans," Proceedings of ASME Turbo Expo 2014: Turbine Technical Conference and Exposition, Jun. 2014, pp. V01AT10A027.
[7] F. Mendonca, A. Read, V. G. Silva, and F. H. J. Imada, "Efficient CFD simulation process for aero acoustic driven design," SAE Technical Paper 2010-36-0545, October 2010.
[8] C. Schram, "Aboundary element extension of Curle's analogy for non-compact geometries at low-March number," Journal of Sound and Vibration, vol. 322, pp. 264-281, 2009.
[9] D. W. Wundrow and A. Khavaran, "On the applicability of high-frequency approximations to Lilley's equation," Journal of Sound and Vibration, vol. 272, pp. 793-830, 2004.
[10] T. O. Imano, Y. Hiraguri, and Y. Kamoshida, "Linearized Eurle simulations of sound propagation with wind effects over a reconstructed urban terrain using digital geographic information," Applied Acoustics, vol. 74, pp. 1354-1366, 2013.
[11] S. Sarkar and M.Y. Hussaini, "Computation of the sound generated by isotropic turbulence," NASA Contact Report 191543, ICASE no. 93-74, pp. 1-26, Oct. 1993.
[12] M. Gennaro, and D. Caridi, "Ffowcs Williams- Hawkings acoustic analogy for simulation of NASA SR2 propeller noise in transonic cruise condition," ECCOMAS CFD, 2010.
[13] Q. Gu and C. T. Wang, Noise controlling engineering, 1st ed. Beijing: Coal Industry, 2008. (In Chinese)